

# High Activity of Helical Carbon Nanotube supported Pd Nanoparticles for Ethanol Electro-oxidation in Alkaline Media

Beibei Wang<sup>1</sup>, Rongjing Cui<sup>2</sup>, Zhida Han<sup>2</sup>, Yuhan Zhang<sup>1</sup>, Lin Wang<sup>1,\*</sup>

<sup>1</sup> Department of Medical Chemistry, Hebei Medical University, Shijiazhuang 050017, China

<sup>2</sup> School of Chemistry and Materials Engineering, Changshu Institute of Technology, Changshu 215500, China

\*E-mail: [wanglin\\_hebmu@163.com](mailto:wanglin_hebmu@163.com), [326640539@qq.com](mailto:326640539@qq.com)

Received: 9 October 2018 / Accepted: 28 December 2018 / Published: 7 February 2019

---

Well-dispersed nanoparticles supported on carbon materials are synthesized successfully with a simple and facile method. Poly diallyldimethylammonium chloride (PDDA) functionalized helical carbon nanotubes (HCNTs) were used as the support material for the deposition of Pd nanoparticles by means of chemical reduction. The catalyst was characterized by scanning electron microscopy, transmission electron microscopy, energy dispersive X-ray spectroscopy, X-ray diffraction and X-ray photoelectron spectroscopy. The electrocatalytic activities of the prepared nanocomposites towards ethanol electro-oxidation were studied by cyclic voltammetry and chronoamperometry. The results indicated that Pd nanoparticles, with an average size of 4 nm, were uniformly dispersed onto the HCNTs/PDDA with a metal weight percentage of 20 wt. %. The method provides a new vision for decentralization of the metal nanoparticles upon functionalized carbon supports for application as electrocatalyst in fuel cells.

---

**Keywords:** Pd nanoparticles, Helical carbon nanotubes, Ethanol oxidation

## 1. INTRODUCTION

Direct ethanol fuel cells (DEFCs) are considered one of the most competitive green power sources because of their high theoretical energy density, environmental friendliness and low temperatures [1-3]. Although Pt and Pt-based materials are effective catalysts for the oxidation of ethanol in alkaline media, their application is significantly limited by the high cost and scarcity of Pt in practice [4-6]. To reduce the costs of catalysts, extensive research have been put in this direction to replace Pt-like catalysts by use of Pt-free materials. Among the substitutes, Pd has been intensively studied as a promising alternative electrocatalyst because of its superior electrocatalytic activity towards formic acid, methanol and ethanol oxidation reactions in alkaline conditions [6]. Furthermore, Pd-based catalysts present higher catalytic activity and poisonous tolerance toward ethanol than that of Pt and Pt-based

catalysts in alkaline solution due to a different reaction mechanism [7-10]. As supports for the catalysts in direct fuel cells, various carbon materials have been investigated. The structure and properties of the carbon supports have significant effects on the activity and stability of the catalysts [11, 12]. In these studies, graphene [13, 14], carbon nanotubes [15] and carbon nanofibers [16] play important roles in nanoscience because of its exceptional electrical, mechanical and optical properties. There is a vast amount of research going on for the development of its applications, especially in the field of electrocatalysis and sensors [17].

Helical carbon nanotubes (HCNTs) were first observed in 1994 by Zhang et al [18]. Since then, scientists have directed much effort towards studying of the morphology and physical characteristics of carbon nanohelices, and have suggested potential applications due to their helical structure and unique physical properties [19, 20]. In our previous report, we had shown that the HCNTs have a larger surface area than that of CNTs, which enables an efficient area for the loading of metal particles [21]. In addition, HCNTs naturally contain more graphitic edge defects and edge planes which facilitate functionalization processes [22]. However, HCNTs are easily aggregate through strong van der Waals' and  $\pi$ - $\pi$  interactions, resulting in a discontinuous and nonuniform film [23]. It has been reported that the aggregation of HCNTs can be prevented by ionic liquids through cation- $\pi$  interactions between the ionic liquids and HCNTs. Poly diallyldimethylammonium chloride (PDDA), a linear positively charged polymer, has attracted much research interest owing to the capability of PDDA in effectively stabilizing carbon materials in aqueous phase. Moreover, the strong ionic polymer matrix of PDDA could allow the support material to be further decorated with Pd nanoparticles. This motivated us to investigate the feasibility of incorporating an ionic-polymer support into Pd-based catalyst for direct fuel cells application.

In the present work, we synthesized Pd-based electrocatalyst in the form of HCNTs/PDDA and Pd nanoparticles, which demonstrates excellent catalytic performance and high stability. We prepared HCNTs *via* using Fe particles as the catalyst. After HCNTs were functionalized with PDDA, well-crystallized Pd nanoparticles were successfully deposited onto the surface of the HCNTs *via* a facile method. The adopted techniques of characterization cover SEM, TEM, XRD, EDS, XPS. The catalytic properties of the as-prepared materials towards ethanol electro-oxidation in alkaline media were also studied. In summary, the results show that the electrocatalyst developed in this work is quite promising as the anode for the construction of direct ethanol fuel cells.

## 2. EXPERIMENTAL

### 2.1 Materials and Apparatus

NaOH, KOH, NaBH<sub>4</sub>, FeCl<sub>3</sub>·6H<sub>2</sub>O, PdCl<sub>2</sub>, 1,2-ethylenediamine, ethanol, ethylene glycol, sodium acetate and nafion were purchased from Sinopharm chemical reagent company. Poly (diallyldimethylammonium chloride) (PDDA, MW=200,000~350,000) and Vulcan XC-72(VX-72, 20 wt. % Pd) were obtained from Sigma-Aldrich company. All reagents used are of analytical reagent grade. Double-distilled water was used throughout.

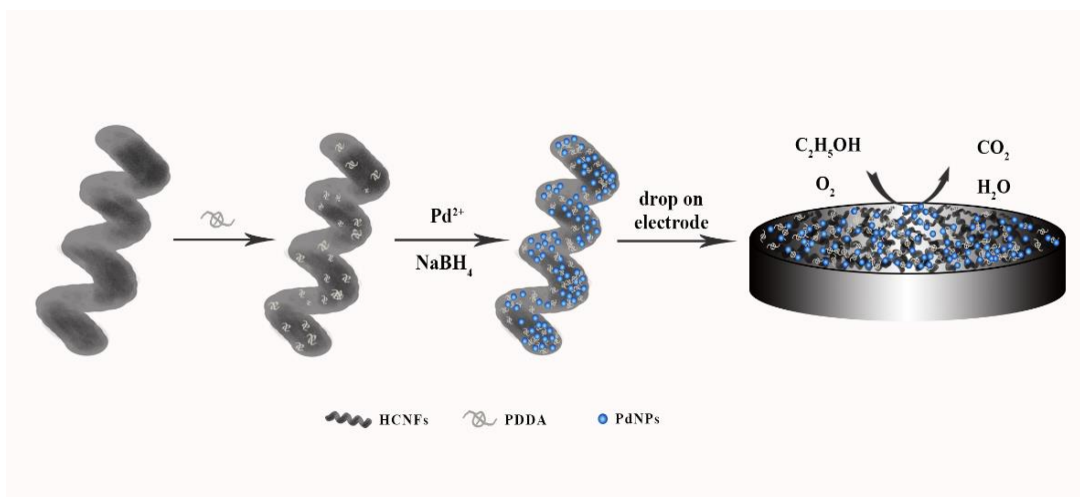
The size and morphology of these prepared samples were observed by a field-emission scanning electron microscope (SEM) and transmission electron microscope (TEM). The crystal phases of these samples were analyzed by X-ray diffraction (XRD) using Cu K $\alpha$  radiation. The elemental states of the catalysts were analyzed by X-ray photoelectron spectroscopy (XPS). All electrochemical experiments were carried out on a CHI 660D workstation. The as-prepared electrocatalyst was the working electrode (GCE, 3mm diameter) and the Pt wire worked as the counter electrode, together with a saturated calomel electrode (SCE) as the reference electrode.

## 2.2 Synthesis of helical carbon nanotubes

High quality HCNTs were synthesized according to a previous report [24]. Briefly, 1.0 g of FeCl<sub>3</sub>·6H<sub>2</sub>O was dissolved in 20 mL of ethylene glycol to form a clear solution, followed by the addition of 3.0 g of NaAc, 0.8 g of NaOH and 10 mL of 1,2-ethylenediamine. These components were homogenized in an ultrasonic bath for 30 min and put in a clean autoclave. The autoclave was heated to and maintained at 200°C for 8 h. The estimated precursors Fe<sub>3</sub>O<sub>4</sub> particles were rinsed with absolute ethanol for 6 times and kept for full drying at 60°C for 12 h. Then, 100 mg of the Fe<sub>3</sub>O<sub>4</sub> was cast on a ceramic plate which was transferred to a reaction tube. The reduction process of Fe<sub>3</sub>O<sub>4</sub> was performed under hydrogen atmosphere at 425°C with 4 h holding time. Finally, pyrolysis of acetylene at 425°C was maintained for 1 h on the reduced Fe catalyst. The HCNTs was collected once cooled to room temperature.

## 2.3 Preparation of Pd/HCNTs/PDDA nanocomposites

Scheme 1 depicts the procedure for the preparation of Pd/HCNTs/PDDA. A certain amount of HCNTs were dispersed into 0.20% PDDA solution by an ultrasonic emitter with power of 300 W at 60 Hz for 20 min at room temperature. Residual PDDA was rinsed with water several times.



**Scheme 1.** Typical procedure for the synthesis of the Pd/HCNTs/PDDA

14 mg of functionalized HCNTs/PDDA and 670  $\mu\text{L}$  of  $\text{PdCl}_2$  solution (38.6 mM) were mixed in 20 ml of ultrapure water. The suspensions were stirred for 1 h, followed by the dropwise addition of excess  $\text{NaBH}_4$  solution [25]. Later on, the product was centrifuged at the rotation rate of 9000 r/min and rinsed with deionized water several times. The collected black solid was dried under vacuum at  $70^\circ\text{C}$ . The palladium loading of the catalyst was 20 wt. %. 5  $\mu\text{L}$  of the catalytic ink was deposited on the clean glassy carbon electrodes and dried at room temperature. Finally, 3  $\mu\text{L}$  of 0.05% Nafion solution was transferred on the surface of electrodes. As comparison, the commercial catalyst Pd/VX-72 was prepared under the same conditions.

### 3. RESULTS AND DISCUSSION

#### 3.1 Characterization

As shown in Figure 1A and C, the majority of the obtained HCNTs clearly show that two helical segments with the same length often symmetrically grew from two sides of a catalytic particle with an average diameter of 80~100 nm. Figure 1B and D shows SEM and TEM images of Pd/HCNTs/PDDA at different magnifications. Uniform dispersion of Pd nanoparticles on the surface of HCNTs in Pd/HCNTs/PDDA electrocatalyst was observed from the images. It can be seen that the nano-sized particles of Pd were highly deposited onto the surface of the HCNTs, with an average size of about 4 nm, exhibit similar morphologies in terms of grain size and distribution. The particle size distribution also shows a relatively narrow distribution ranging from 2.5 nm to 6 nm with a mean value of ca. 3 nm (Figure 1E), which is consistent with the results of the TEM image presented. Overall, the intimate contact of HCNTs with non-covalent PDDA facilitates uniform distribution of Pd nanoparticles on the surface result in more catalytically active sites for electrocatalytic reaction [26]. The corresponding energy dispersive X-ray (EDS) analysis showed that the species supported on the HCNTs was Pd element (Figure 1F). In summary, these results indicated that Pd/HCNTs/PDDA nanocomposites were successfully synthesized. However, in order to obtain the more suitable scientific data of the Pd nanoparticles on the carbon supports, XRD and XPS investigations were carried out.

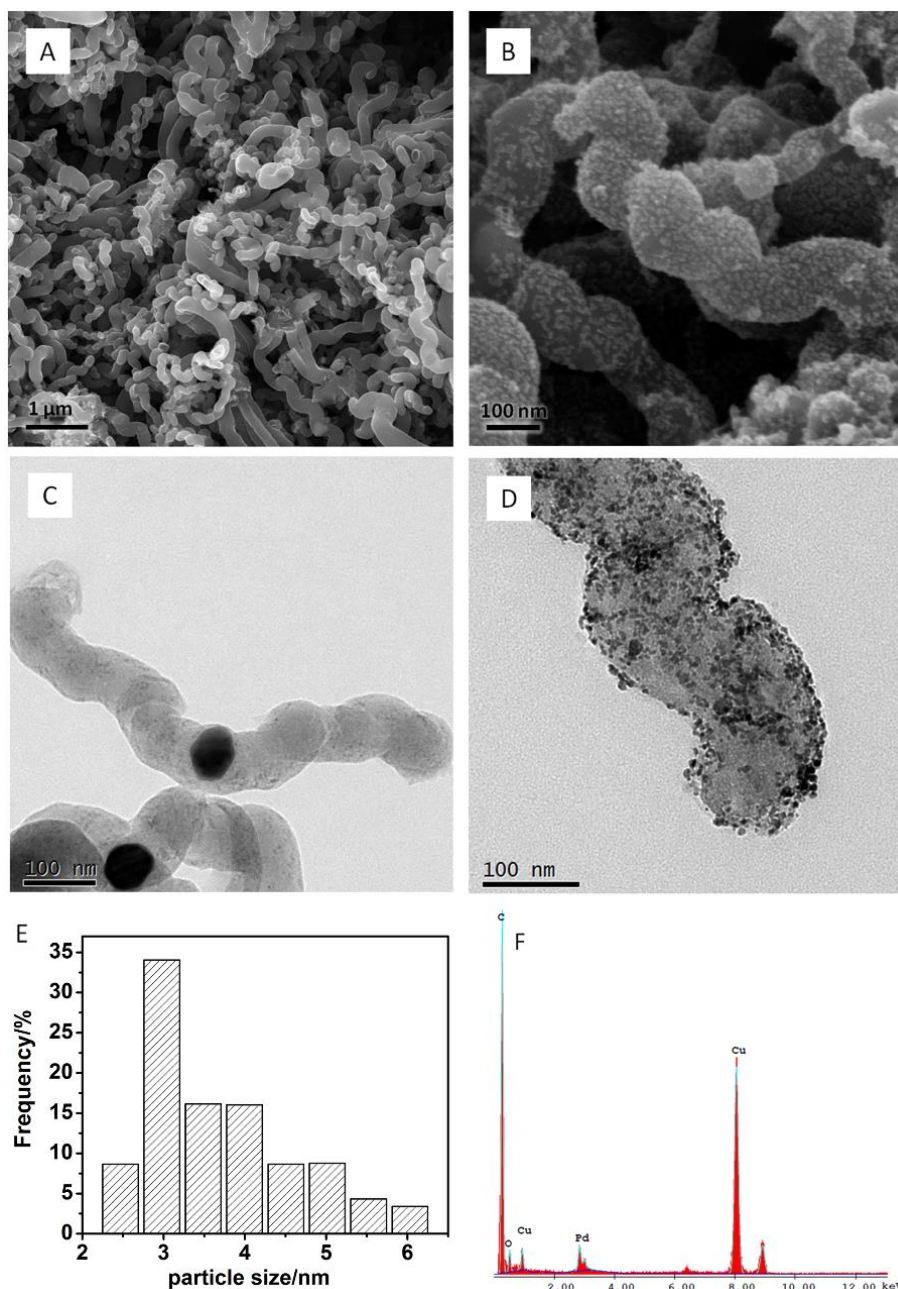


**Figure 1.** SEM of HCNTs (A) and Pd/HCNTs/PDDA (B), TEM of HCNTs (C) and Pd/ HCNTs/PDDA (D), Histogram of particle size distribution of Pd/HCNTs/PDDA (E) and EDS analysis of the Pd/HCNTs/PDDA (F)

Figure 2 shows the XRD profiles of HCNTs, together with the Pd/HCNTs/PDDA composites. For all the samples, the initial peak at a  $2\theta$  value of  $25.9^\circ$  and is referred to carbon (002) plane originates from carbon supports [27]. Meanwhile, the tiny diffraction peaks from  $37.3^\circ$  to  $49^\circ$  can be indexed to the  $\text{Fe}_3\text{C}$  from Fe and carbon in the synthesis of the HCNTs. The strong peaks at  $39.5^\circ$ ,  $45.9^\circ$ ,  $67.1^\circ$ ,  $80.0^\circ$  can be attributed to the diffraction peaks of Pd crystal face (111), (200), (220) and (311), respectively, indicating the presence of Pd nanoparticles in the composites and have single face structure [28]. However, there were no other distinct reflection peaks, demonstrating the high purity of the Pd/HCNTs/PDDA nanocomposites.

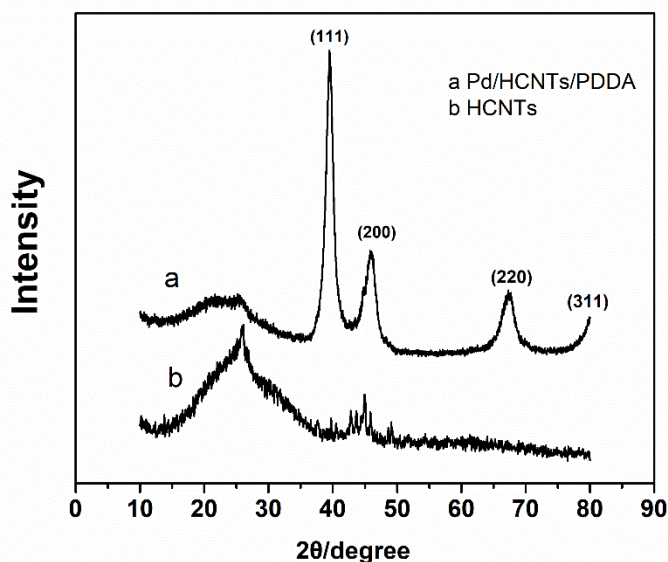


**Figure 2.** XRD patterns of HCNTs and Pd/HCNTs/PDDA

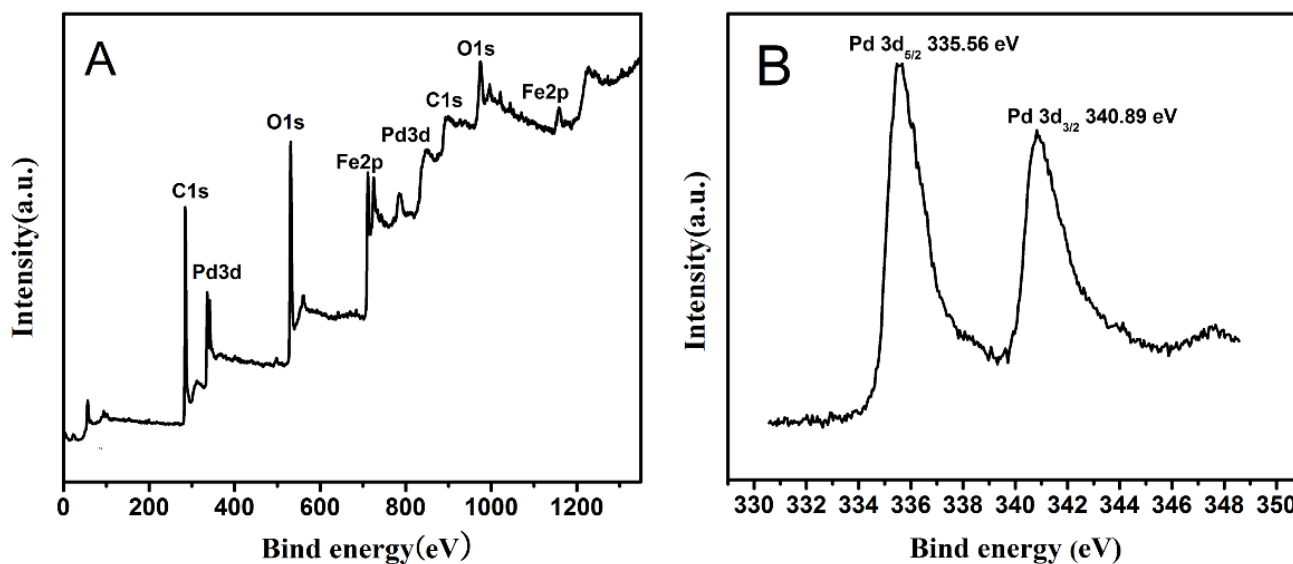


**Figure 3.** XPS survey spectra of Pd/HCNTs/PDDA (A) and the XPS spectrum for Pd 3d regions (B) of Pd/HCNTs/PDDA

The electronic states and surface characteristics of the catalysts were investigated by X-ray photoelectron spectroscopy (XPS). The full-scale XPS spectrum in Figure 3A not only reveals the presence of the C 1s peak at 284.4 eV and the O 1s peak at 532.2 eV, but also shows Fe 2p and Pd 3d elemental peaks in the catalyst. Figure 3B shows the Pd 3d XPS spectrum of the Pd/HCNTs/PDDA composites, in which two peaks at binding energies of 335.56 eV and 340.89 eV are ascribed to metallic Pd 3d<sub>5/2</sub> and Pd 3d<sub>3/2</sub> [29]. Through the analysis of SEM, TEM, XRD and XPS spectra of the Pd/HCNTs/PDDA, it could be confirmed that the Pd nanoparticles were successfully dispersed onto the surface of HCNTs.

## 3.2 Electrochemical analysis

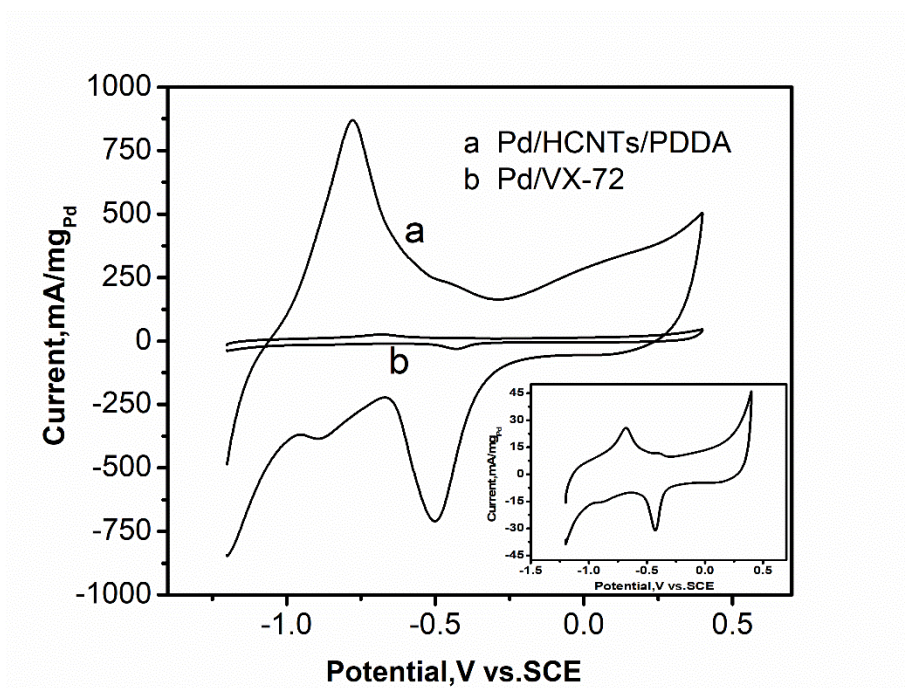


**Figure 4.** CV curves of the Pd/HCNTs/PDDA and Pd/VX-72 modified electrodes in nitrogen bubbled 1 M KOH with a sweep rate of  $50 \text{ mV s}^{-1}$ . Inset: CV curve of Pd/VX-72 catalyst

The cyclic voltammograms of the Pd/HCNTs/PDDA and Pd/VX-72 catalysts were measured in 1.0 M KOH and the results are shown in Figure 4. The peaks in the region between -1.0 V and 0.8 V can be attributed to the adsorption and desorption of hydrogen. With the scans moving towards the high potential region, oxidation peaks appear due to the formation of surface oxides and, subsequently, the peaks corresponding to the reduction of the oxides show up during the negative scans. The electrochemically active surface area (ESA) of the samples can be measured from the area of the reduction peak of PdO which is an excellent index for the assessment of active sites of the catalysts in accordance with the following equation:

$$E=Q/SL$$

where S is the proportionality constant used to relate charge with area and L is the catalyst loading in g. A charge value of  $405 \mu\text{C cm}^{-2}$  is assumed for the reduction of the PdO monolayer. Table 1 shows the calculated ESA values which are in the following order:  $\text{ESA}_{(\text{Pd}/\text{HCNTs}/\text{PDDA} \text{ modified electrode})} > \text{ESA}_{(\text{Pd}/\text{VX-72} \text{ modified electrode})}$ . Quantitatively, the ESA of the Pd/HCNTs/PDDA electrocatalyst was approximately 34.7 times larger than that of the Pd/VX-72 electrocatalyst. Uniform distribution of palladium nanoparticles could account for increased ESA values in contrast to that of Pd/VX-72 [30]. Moreover, compared with Pd/VX-72 catalyst, the 3D-helical and porous structure of HCNTs can provide more active reaction centers for electrons and molecules, which may facilitate the reaction kinetics on the modified electrode surface [31].

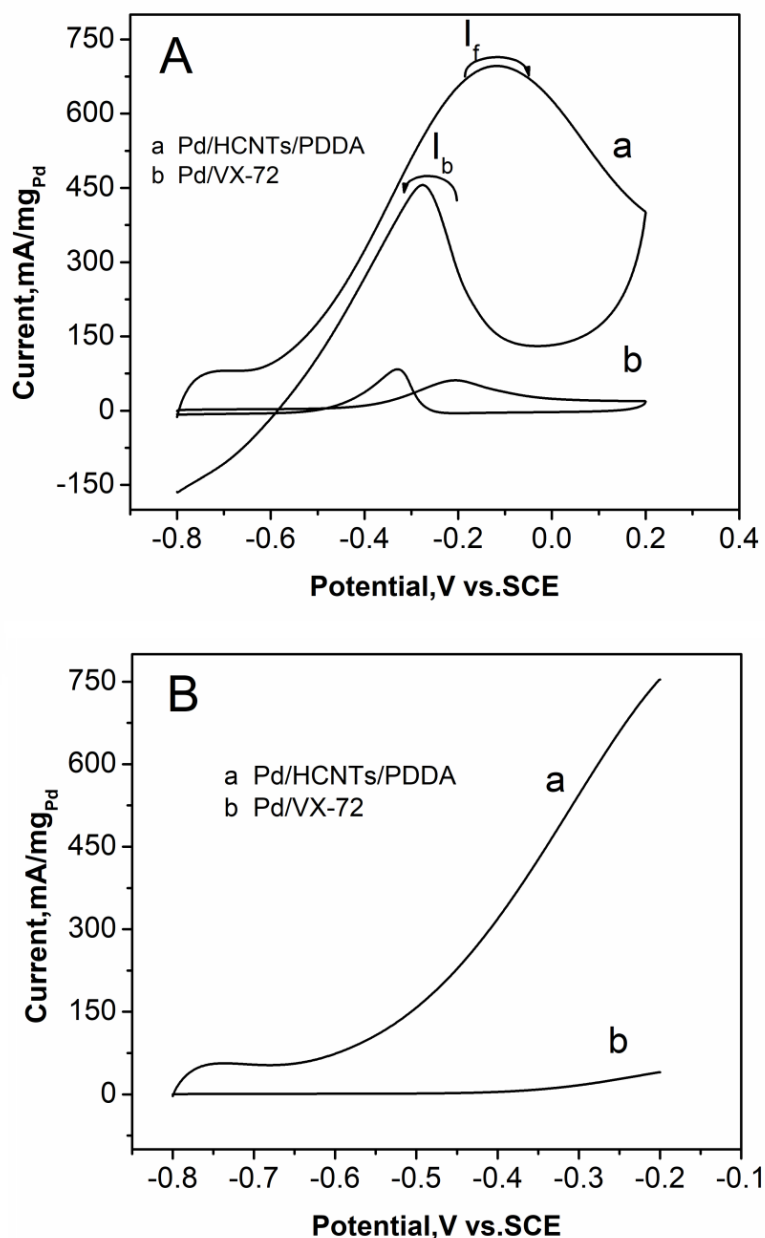


**Figure 5.** CV curves (A) and LSV curves (B) of the Pd/HCNTs/PDDA and Pd/VX-72 obtained in nitrogen bubbled 0.1 M KOH in presence of 1.0 M ethanol with a sweep rate of 50 mV s<sup>-1</sup>

The electrocatalytic performance of the Pd/HCNTs/PDDA catalyst for ethanol oxidation was evaluated in a mixed solution of 0.1 M KOH and 1.0 M ethanol at room temperature by cyclic voltammetry (see Figure 5A) and linear sweep voltammetry (see Figure 5B). All curves show two anodic peaks, a forward peak and a backward peak. Generally, the forward peak current represents the oxidation of the freshly chemisorbed species that result from ethanol adsorption, whereas the backward peak current corresponds to the removal of incompletely oxidized species that have accumulated on the catalyst surface during the forward scan. The peak current density normalized by the loading of Pt metal was defined as the mass activity to evaluate the catalytic activity toward ethanol electrooxidation. From Figure 5A and B, the onset potential for the Pd/HCNTs/PDDA catalyst is about -0.56 V, whereas the

onset potential for the Pd/VX-72 catalyst is located at  $-0.46$  V, suggesting that the oxidation of ethanol is easier to accomplish with the Pd/HCNTs/PDDA catalyst. As shown in Figure 5A, the current density of the Pd/HCNTs/PDDA catalyst is approximately  $695.1 \text{ mA mg}^{-1}$ , nearly 11.4 times more than that of the Pd/VX-72 catalyst. An oxidation peak appeared at  $-0.28$  V in the back sweep is mainly assigned to the oxidation of intermediate products that are not entirely oxidized [32, 33]. The electrocatalytic performances of the nanocomposites Pd/HCNTs/PDDA as well as Pd/VX-72 are summarized in Table 1. Based on the above results, ethanol oxidation peak current density at Pd/HCNTs/PDDA electrocatalyst was higher than that at Pd/VX-72, which revealed that the incorporation of palladium nanoparticles and HCNTs greatly enhanced its electrocatalytic performance for ethanol oxidation in KOH solution.

**Table 1.** Comparison of CV results of the different catalyst electrodes

Catalyst	ESA ( $\text{m}^2 \text{ g}^{-1}$ )	$E_{\text{onset}}$ (V)	$I_f$ ( $\text{mA mg}^{-1}$ )	$I_b$ ( $\text{mA mg}^{-1}$ )	$I_f/I_b$
Pd/HCNTs/PDDA	451.3	-0.56	695.1	454.8	1.52
Pd/VX-72	13.0	-0.46	61.1	82.4	0.74

In general, the ratio of forward peak current to backward peak current ( $I_f/I_b$ ) usually imply the electrocatalyst tolerance to carbonaceous intermediates accumulation. As shown in Table 1, the ( $I_f/I_b$ ) ratio of Pd/HCNTs/PDDA is 1.52, which is higher than Pd/VX-72 (0.74), indicating that the as-prepared catalyst effectively enhances the complete oxidation of ethanol to  $\text{CO}_2$ , and fewer CO-like carbonaceous species accumulate on the electrode surface [34]. High catalytic activity of as-prepared Pd/HCNTs/PDDA catalyst can be related to its unique structure. Helical structure allows the ethanol molecules to penetrate through the open pore and reach to the active sites easily and that the nanostructure increase accessible surface area and catalytic active sites.

Chronoamperometry under constant potential at  $-0.1$  V, operated in  $0.1 \text{ M}$  KOH aqueous solution containing  $1.0 \text{ M}$  high purity ethanol for  $2000 \text{ s}$  is to evaluate the durability of these catalysts. As shown in Figure 6, in the beginning the potentiostatic currents decreased rapidly for all catalysts due to the formation of double layer capacitance. The following current decrease should originate from the loss of surface active sites caused by the adsorption of intermediate species on the catalyst surface [35]. However, the current density at Pd/HCNTs/PDDA is higher and decreases more slowly compared with that at Pd/VX-72 catalyst. At the end of the measurement, the oxidation current on the Pd/HCNTs/PDDA modified electrode is considerably higher than that of Pd/VX-72, which can be clearly observed in the curves. This result suggests that the support material HCNTs/PDDA and the Pd nanoparticles enhance the electrocatalytic activity and stability of the catalyst. Compared with the other catalysts in literatures, the prepared catalyst in this work has good electrocatalytic activity. More details for the ethanol oxidation are summarized in Table 2.

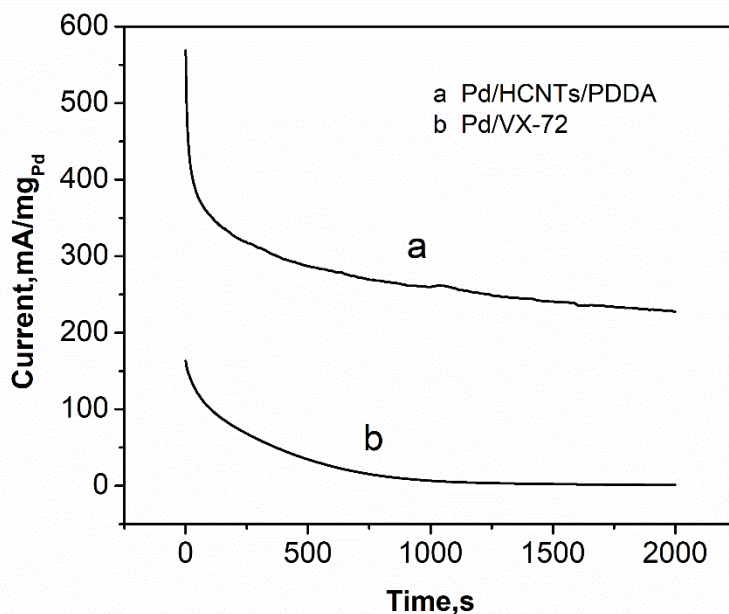


**Figure 6.** CHA curves of the Pd/HCNTs/PDDA and Pd/VX-72 measured in nitrogen bubbled 0.1 M KOH in presence of 1.0 M ethanol with a sweep rate of  $50 \text{ mV s}^{-1}$

**Table 2.** Comparison of electrocatalytic activity with different catalysts

Catalyst	Specific activity ( $\text{mA cm}^{-2}$ )	Mass activity ( $\text{mA mg}^{-1}$ )	ESA ( $\text{m}^2 \text{g}^{-1}$ )	$E_p$	Ref.
Pd-rGO hybrids	1.11	42.16	3.7	-0.174	[36]
Pd-NrGO hybrids	0.51	32.76	6.3	-0.112	[36]
PtPd/PDA-rGO	—	281.5	352.1	0.130	[37]
Pd/P-C	1.1	325	—	-0.12	[38]
Pd/HCNTs/PDDA	19.5	695.1	451.3	-0.122	This work

#### 4. CONCLUSIONS

In this study, we introduced a simple and facile method to prepare Pd nanoparticles on PDDA-functionalized helical carbon nanotubes for the electro-oxidation of ethanol. The nano-sized particles of Pd, with a diameter of approximately 4 nm, were uniformly deposited in high numbers onto the surface of the HCNTs. The nanocomposites Pd/HCNTs/PDDA greatly enhanced the electrocatalytic activity and stability towards ethanol, which could be attributed to the following: (1) The 3D-helical and porous structure of HCNTs can provide more active reaction centers for electrons and molecules. (2) The high

dispersion nanoparticles in Pd/HCNTs/PDDA can cause high specific surface area and exposing sufficient catalytic sites. These results confirmed that Pd/HCNTs/PDDA catalyst synthesized in this work is a favorable candidate for alkaline direct ethanol fuel cells.

#### ACKNOWLEDGEMENTS

We greatly appreciate the support of the National Natural Science Foundation of China (51371004), Major Natural Science Foundation of Jiangsu Provincial Education Department (16KJA150007), Undergraduate innovative experimental program(USIP2018210).

#### References

1. Y.Y. Liang, Y.G. Li, H.L. Wang and H.J. Dai, *J. Am. Chem. Soc.*, 135 (2013) 2013.
2. H.J. Huang and X. Wang, *J. Mater. Chem. A*, 2 (2014) 6266.
3. X.X. Zhao, W.X. Yuan, Q.X. Wu, H.Y. Sun, Z.K. Luo and H.D. Fu, *J. Power. Sources*, 273 (2015) 517.
4. Y.Y. Huang, J.D. Cai and Y.L. Guo, *Appl. Catal. B. Environ.*, 129 (2013) 549.
5. S. Sun, Z. Jusys and R.J. Behm, *J. Power. Sources*, 231 (2013) 122.
6. J.S. Wang, N.C. Cheng, M.N. Banis, B.W. Xiao, A. Riese and X.L. Sun, *Electrochim. Acta*, 185 (2015) 267.
7. M. Laskar and S.E. Skrabalak, *ACS Catal.*, 4 (2014) 1120.
8. V. Divya, S. Mondal and M.V. Sangaranarayanan, *J. Nanosci. Nanotechno.*, 19 (2019) 758.
9. J.B. Ding, L.Z. Bu, S.J. Guo, Z.P. Zhao, E.B. Zhu, Y. Huang and X.Q. Huang, *Nano. Lett.*, 16 (2016) 2762.
10. M. Laskar and S.E. Skrabalak, *J. Mater. Chem. A*, 4 (2016) 6911.
11. Y.C. Park, H. Tokiwa, K. Kakinuma, M. Watanabe and M. Uchida, *J. Power. Sources*, 315 (2016) 179.
12. V. Celorrio, J.F. Montano, R. Moliner, E. Pastor and M.J. Lazaro, *Int. J. Hydrog. Energy*, 39 (2014) 5371.
13. L.N. Gao, W.B. Yue, S.S. Tao and L.Z. Fan, *Langmuir*, 29 (2013) 957.
14. H. Rostami, A.A. Rostami and A. Omrani, *Electrochim. Acta*, 194 (2016) 431.
15. M.S. Ahmed and S. Jeon, *J. Power. Sources*, 282 (2015) 479.
16. Y. Oh, S.K. Kim, D.H. Peck, J.S. Jang, J. Kim and D.H. Jung, *Int. J. Hydrog. Energy*, 39 (2014) 15907.
17. D. Hiltrop, J. Masa, A. Maljusch, W. Xia, W. Schuhmann and M. Muhler, *Electrochem. commun.*, 63 (2016) 30.
18. X.B. Zhang, X.F. Zhang, D. Bernaerts, G.V. Tendeloo, S. Amelinckx, J.V. Landuyt, V. Ivanov, J.B. Nagy, P. Lambin and A.A. Lucas, *Euro. Phys. Lett.*, 27 (1994) 141.
19. J.G. Gibbs, A.G. Mark, T.C. Lee, S. Eslami, D. Schamel and P. Fischer, *Nanoscale*, 6 (2014) 9457.
20. V. Bajpai, L.M. Dai and T. Ohashi, *J. Am. Chem. Soc.*, 126 (2004) 5070.
21. L. Wang, L. Mei, X. Liu, J.K. Shi, Y. H. Li, N. Gu and R.J. Cui, *Microchim. Acta*, 182 (2015) 1661.
22. M. Nasserri, D.P. Hunley, A. Sundararajan, M.J. Boland and D.R. Strachan, *Carbon*, 77 (2014) 958.
23. B.Y. Zhang, D.K. Huang, X.B. Xu, G. Alemu, Y.B. Zhang, F. Zhang, Y. Shen and M.K. Wang, *Electrochim. Acta*, 91 (2013) 261.
24. S.B. Zhang, Y.M. Shen, G.Y. Shen, S. Wang, G.L. Shen and R.Q. Yu, *Anal. Biochem.*, 494 (2016) 10.
25. Y.F. Fan, Y.C. Zhao, D.H. Chen, X. Wang, X.L. Peng and J.N. Tian, *Int. J. Hydrog. Energy*, 40 (2015) 322.
26. H. Biuck and S. Mohammadyari, *Int. J. Hydrog. Energy*, 40 (2015) 10833.
27. N.J. Tang, J.F. Wen, Y. Zhang, F.X. Liu, K.J. Lin and Y.W. Du, *ACS Nano.*, 4 (2010) 241.
28. R.J. Cui, N. Gu, J.K. Shi, Z.D. Han, P. Guo, J. Xu and G.H. Zhang, *Electrochim. Acta*, 147 (2014) 778.

29. Y.T. Zhang, H.H. Shu, G. Chang, K. Ji, M. Oyama, X. Liu and Y.B. He, *Electrochim. Acta*, 109 (2013) 570.
30. F.C. Zhu, G.S. Ma, Z.C. Bai, R.Q. Huang, B. Tang, Z.H. Zhang and X.G. Wang, *J. Power. Sources*, 242 (2013) 610.
31. G.Z. Hu, F. Nitze, T. Sharifi, H.R. Barzegar and T. Wagberg, *J. Mater. Chem.*, 22 (2012) 8541.
32. C.X. Xu, L.Q. Wang, R.Y. Wang, K. Wang, Y. Zhang, F. Tian and Y. Ding, *Adv. Mater.*, 21 (2009) 2165.
33. X.G. Wang, B. Tang, X.B. Huang, Y. Ma and Z.H. Zhang, *J. Alloy. Compd.*, 565 (2013)120.
34. J.J. Shi, G.H. Yang and J.J. Zhu, *J. Mater. Chem.*, 21 (2011) 7343.
35. Y.H. Li, Q.Z. Xu, Q.Y. Li, H.Q. Wang, Y.G. Huang and C.W. Xu, *Electrochim. Acta*, 147 (2014)151.
36. R. Kumar, E. Silva, R.K. Singh, R. Savu, A.V. Alaferdov, L.C. Fonseca, L.C. Carossi, A. Singh, S. Khandka, K.K. Kar, O.L. Alves, L.T. Kubota and S.A. Moshkalev, *J. Colloid. Interf. Sci.*, 515 (2018) 160.
37. S. Themsirimongkon, K. Ounnunkad and S. Saipanya, *J. Colloid. Interf. Sci.*, 530 (2018) 98.
38. J.C.M. Silva, I.C. Freitas, A.O. Neto, E.V. Spinace and V.A. Ribeiro, *Ionics*, 24 (2018) 1111.

© 2019 The Authors. Published by ESG ([www.electrochemsci.org](http://www.electrochemsci.org)). This article is an open access article distributed under the terms and conditions of the Creative Commons Attribution license (<http://creativecommons.org/licenses/by/4.0/>).